International Journal of Electrical and Computer Engineering (IJECE)
Vol. 16, No. 1, February 2026, pp. 121~134
ISSN: 2088-8708, DOI: 10.11591/ijece.v16i1.pp121-134

An enhanced improved adaptive backstepping–second-order sliding mode hybrid control strategy for high-performance electric vehicle drives

Huu Dat Tran, Ngoc Thuy Pham
Department of Electrical Engineering Technology, Industrial University of Ho Chi Minh City, Ho Chi Minh, Vietnam

Article Info

Article history:

Received Jun 26, 2025
Revised Sep 24, 2025
Accepted Nov 23, 2025

Keywords:

Backstepping
Electric vehicle
Field oriented control
Second order sliding mode
Six phase induction motor
Variable gain super twisted algorithm

ABSTRACT

This paper proposes an enhanced hybrid speed control strategy, termed improved adaptive backstepping–second-order sliding mode (IABSSOSM), for six-phase induction motor (SPIM) drives in electric vehicle (EV) propulsion systems. The proposed method combines the systematic design framework of Backstepping in the outer speed and flux loops with a second-order sliding mode controller in the inner current loop. An innovation of the approach is the integration of a variable-gain super-twisting algorithm (VGSTA), which dynamically adjusts the control effort based on disturbance levels, thereby minimizing chattering and enhancing robustness against system uncertainties. To further improve disturbance rejection, a predictive torque estimator is incorporated using a forward Euler discretization, enabling accurate torque prediction and proactive compensation. This hybrid structure significantly improves convergence speed, enhances reference speed tracking accuracy, and ensures fast and precise torque response, and its strong resilience to external load disturbances, system parameter variations enable stable and reliable operation under challenging conditions. The effectiveness of the proposed approach is validated through comprehensive simulations using the MATLAB/Simulink.

Corresponding Author:

Ngoc Thuy Pham
Department of Electrical Engineering Technology, Industrial University of Ho Chi Minh City
12 Nguyen Van Bao Street, ward 4, Go Vap District, 700000, Ho Chi Minh, Vietnam
Email: ngocpham1020@gmail.com

1. INTRODUCTION

In recent years, in response to the greenhouse effect and the depletion of fossil fuel resources, numerous studies have focused on developing high-efficiency drive systems for electric vehicles (EVs) as a sustainable solution for energy and environmental challenges. The electric drive system is one of the key components of an EV [1]–[3]. EVs using electric motors are not only environmentally friendly but also capable of delivering fast, accurate, and safe torque responses. It plays a crucial role in EV performance, particularly in ensuring torque accuracy, efficiency, and reliability [1]–[5]. The EV drive system typically consists of three main components: an electric motor, a power converter, and a controller. Among these, the motor must meet driver-defined torque and speed requirements. Notably, among various motor technologies, the six-phase induction motor (SPIM) has gained increasing attention for EV applications due to its superior characteristics such as fault tolerance, higher torque density, reduced current per phase, lower torque ripple, and improved reliability [6], [7]. These features make SPIMs well-suited for safety-critical and performance-

sensitive EV platforms. However, the complexity of SPIM dynamics necessitates the development of advanced control strategies beyond traditional linear methods.

Several advanced control strategies have been investigated to exploit the features of this motor, including field-oriented control (FOC), direct torque control (DTC), and model predictive control (MPC) [8]–[11]. Among these, both DTC and MPC require optimal voltage vector selection and become increasingly complex with a higher number of stator phases of SPIM. Opposite, FOC remains dominant due to its balance between performance and implementation simplicity. However, traditional FOC using linear PID controllers often lacks robustness under parameter variation and external disturbances [12]–[14].

Nevertheless, traditional FOC strategies that rely on proportional-integral-derivative (PID) controllers often fall short of the high-performance demands in EV systems. To overcome this limitation, several nonlinear control methods have been researched as alternatives to PID, such as sliding mode control, backstepping, fuzzy logic, neural networks, passive control, predictive control, and Hamiltonian control [15]–[23]. However, these techniques typically require accurate mathematical models and involve complex computation. When applied independently, they may not achieve optimal results, especially in nonlinear systems. Such as, backstepping (BS) and sliding mode control (SMC), each offering advantages in stability analysis and robustness, respectively. Yet, each approach has known drawbacks: BS is sensitive to uncertainties, while SMC introduces chattering effects. As a result, integrating multiple control techniques to leverage their respective strengths has become a promising research direction for improving the performance of AC motor drives [24]–[29]. In [29], a hybrid backstepping-sliding mode (BS-SM) control structure was proposed, demonstrating a promising approach for motor drives. It is easy to see that, while backstepping provides a systematic framework for stability analysis, its performance degrades significantly in the presence of parameter uncertainties, such as variations in rotor resistance and vehicle inertia, and although conventional sliding mode control offers excellent robustness against such uncertainties, it inherently suffers from the high-frequency chattering phenomenon, which can excite unmodeled dynamics and damage the actuator. The challenge of chattering and the lack of adaptivity under time-varying load conditions remain due to existing implementations often use fixed gains or neglect real-time disturbance estimation, leading to limitations in adaptability, excessive control effort, or degraded performance in practical EV scenarios.

To address these challenges, this paper proposes a novel control strategy, termed improved adaptive backstepping–second-order sliding mode (IABSSOSM), which incorporates a variable gain super-twisting algorithm (VGSTA) in both speed and current loops. This VGSTA proposed structure dynamically adjusts the control gains based on disturbance estimates, thereby maintaining finite-time convergence and robustness while effectively reducing chattering without requiring prior knowledge of disturbance bounds. Moreover, a predictive torque estimator based on the forward Euler discretization of the SPIM model to proactively handle external load variations also is proposed. This estimator enhances system response by anticipating torque demands and disturbance effects, improving transient performance and overall system robustness.

The performance and robustness of the proposed control scheme for a SPIM drive in EV applications, particularly in terms of stability, response speed, and disturbance rejection, are validated via extensive simulations under standardized EV driving cycles (ECE-40, ECE-15), step speed commands, and load disturbances. Results confirm its superiority over conventional techniques in terms of tracking accuracy, robustness, and dynamic response. The paper is organized as follows: section 2 presents the SPIM drive system model. Section 3 introduces the proposed STABS_PCH controller and resistance/flux estimators. Section 4 discusses the simulation results. Finally, conclusions are drawn in section 5.

2. MODELING OF SPIM DRIVE AND EV PROPULSION SYSTEM

2.1. SPIM drive system modeling

The drive system considered in this study includes a SPIM powered by a six-phase voltage source inverter (SPVSI). The overall structure of the SPIM drive system is illustrated in Figure 1. The vector space decomposition (VSD) technique is used to transform the six-dimensional space into three two-dimensional subspaces in the stationary reference frame. The transformation is performed using a 6×6 transformation matrix as developed in previous literature [1].

$$T_6 = \frac{1}{3}\begin{bmatrix} 1 & -\frac{1}{2} & -\frac{1}{2} & \frac{\sqrt{3}}{2} & -\frac{\sqrt{3}}{2} & 0 \\ 0 & \frac{\sqrt{3}}{2} & -\frac{\sqrt{3}}{2} & \frac{1}{2} & \frac{1}{2} & -1 \\ 1 & -\frac{1}{2} & -\frac{1}{2} & -\frac{\sqrt{3}}{2} & \frac{\sqrt{3}}{2} & 0 \\ 0 & -\frac{\sqrt{3}}{2} & \frac{\sqrt{3}}{2} & \frac{1}{2} & \frac{1}{2} & -1 \\ 1 & 1 & 1 & 0 & 0 & 0 \\ 0 & 0 & 0 & 1 & 1 & 1 \end{bmatrix} \quad (1)$$

The mathematical equations of the SPIM in the stationary reference frame are written as (2):

$$[V_s] = [R_s][I_s] + p([L_{ss}][I_s] + [L_{sr}][I_r])$$
$$[0] = [R_r][I_r] + p([L_{rr}][I_r] + [L_{rs}][I_s]) \quad (2)$$

where $[V], [I], [R], [L]$, and $[Lm]$ represent the voltage, current, resistance, self-inductance, and mutual inductance vectors, respectively. P is the differential operator. Subscripts r and s denote rotor and stator components, respectively. Since the rotor is squirrel-cage type, $[Vr]$ equals zero. The electromechanical energy conversion only occurs in the D–Q subspace:

$$\begin{bmatrix} V_{sD} \\ V_{sQ} \\ 0 \\ 0 \end{bmatrix} = \begin{bmatrix} R_s + PL_s & 0 & PL_m & 0 \\ 0 & R_s + PL_s & 0 & PL_m \\ PL_m & \omega_r L_m & R_r + PL_r & \omega_r L_r \\ -\omega_r L_m & PL_m & -\omega_r L_m & R_r + PL_r \end{bmatrix} \begin{bmatrix} I_{sD} \\ I_{sQ} \\ I_{rD} \\ I_{rQ} \end{bmatrix} \quad (3)$$

among the three subspaces, only the D–Q subspace contributes to torque production [1]. The remaining x–y and z1–z2 subspaces cause power loss and do not participate in energy conversion, hence they are excluded from the control design. Therefore, the SPIM control system can be reduced to a form similar to the D–Q model of a conventional induction motor. However, designing controllers in the stationary reference frame is challenging. To overcome this, the SPIM model is transformed into a synchronous rotating reference frame (dq-frame), which converts current signals into DC components, thereby simplifying control and enhancing speed and torque tracking accuracy.

The transformation from the DQ to dq frame is performed using the transformation matrix T2 defined as (4):

$$T_2 = \begin{bmatrix} \cos(\delta_r) & -sin(\delta_r) \\ sin(\delta_r) & \cos(\delta_r) \end{bmatrix} \quad (4)$$

where δ_r is the rotor angular position with respect to the stator, as shown in Figure 1.

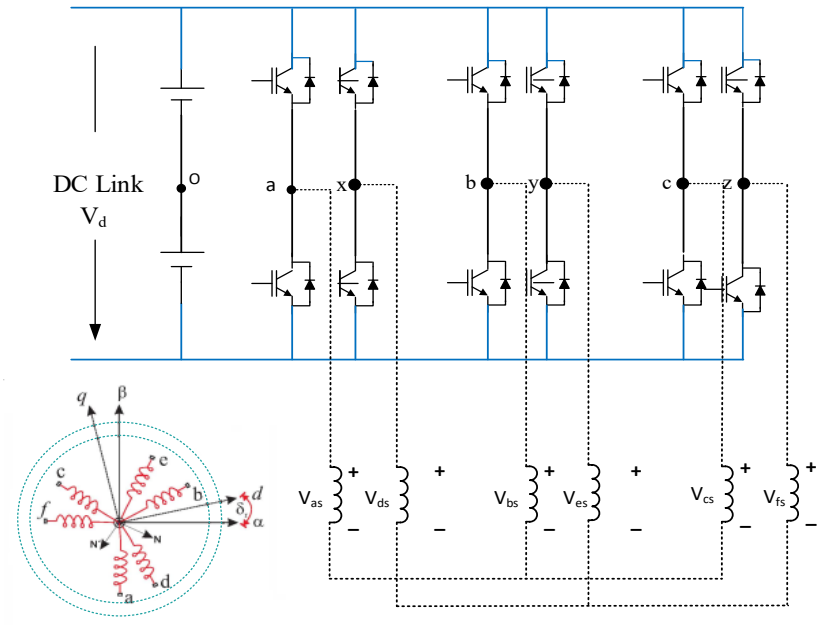

Figure 1. Overall structure of the SPIM drive system

2.2. Vehicle propulsion modeling

Under FOC control, $\psi_{rq}=0$, $\psi_{rd}=\psi_{rd}$. The updated dynamic model of the motor is described using the following space vector differential equations:

$$\begin{cases} L_s \frac{di_{sd}}{dt} = -ai_{sd} + L_s\omega_e i_{sq} + bR_r\psi_{rd} + cu_{sd} \\ L_s \frac{di_{sq}}{dt} = -ai_{sq} + L_s\omega_e i_{sd} + b_r\omega_e\psi_{rd} + cu_{sq} \\ \frac{d\omega_r}{dt} = \frac{3}{2}P\frac{\delta\sigma L_s}{J}(\psi_{rd}i_{sq}) - \frac{T_L}{J} - B\omega_r \\ \frac{d\psi_{rd}}{dt} = \frac{L_m}{\tau_r}i_{sd} - \frac{1}{\tau_r}\psi_{rd} \end{cases} \quad (5)$$

where:

$$\sigma = 1 - \frac{L_m^2}{L_s L_r}; \delta = \frac{L_m}{\sigma L_s L_r}; a = \frac{L_m^2 R_r + L_r^2 R_s}{\sigma L_r^2}; b = \frac{L_m^2 R_r}{\sigma L_r^2}; c = \frac{1}{\sigma}; \tau_r = \frac{L_r}{R_r}$$

$$T_e = \frac{3}{2}n_p\frac{L_m}{L_r}\psi_{rd}i_{sq} \quad (6)$$

$$\omega_{sl} = \frac{L_m}{L_r}\psi_{rd}i_{sq} \quad (7)$$

Alternatively, torque can also be expressed through the dynamic equation:

$$T_e = T_L + B\omega_r + J\frac{d\omega_r}{dt} \quad (8)$$

To propel the EV, the SPIM must generate torque for the wheels as performing in Figure 2. This illustrates the proposed transmission diagram in electric vehicle. Key factors influencing the EV's dynamic model include road conditions, inclines, acceleration ability, aerodynamic resistance, etc. The proposed control strategy takes these dynamics into account. The model is based on vehicle mechanics and aerodynamics principles [18]. The total tractive force is given by:

$$\begin{aligned} F_{te} &= F_{rr} + F_{hc} + F_{ad} + F_{la} + F_{wa} \\ &\approx \mu_{rr}mg + mg\sin f + \frac{1}{2}\rho AC_d v^2 + m\frac{dv}{dt} + F_L \end{aligned} \quad (9)$$

where F_{te}: tractive force; F_{rr}: rolling resistance; F_{hc}: hill climbing force; F_{la}: linear acceleration force; F_{wa}: angular acceleration force; m: EV mass; g: gravitational acceleration; v: vehicle speed; μ_{rr}: rolling resistance coefficient; ρ: air density; A: frontal area; Cd: drag coefficient; f: slope angle; FL: external disturbance; r: wheel radius; G: gear ratio; T: required torque; vr: motor speed. In Figure 3, under FOC, the electromagnetic torque T_e is expressed simply as (10):

$$T_m = \frac{rF_{te}}{G} \quad (10)$$

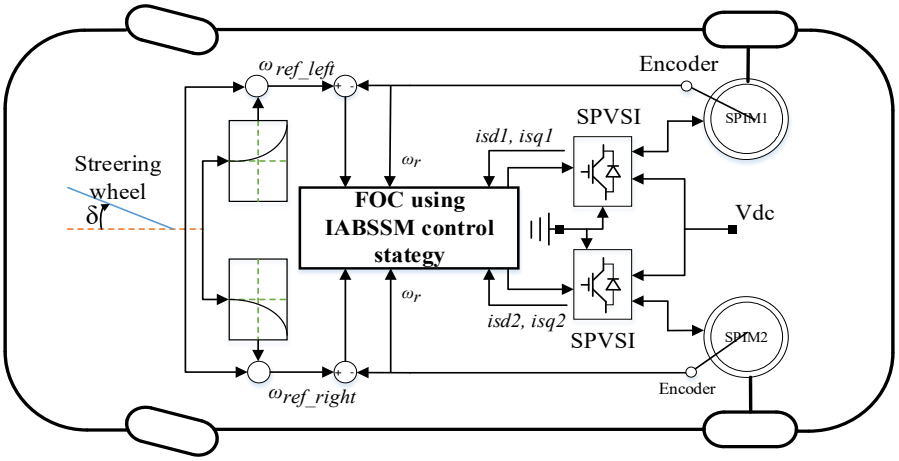

Figure 2. Proposed transmission diagram in electric vehicle

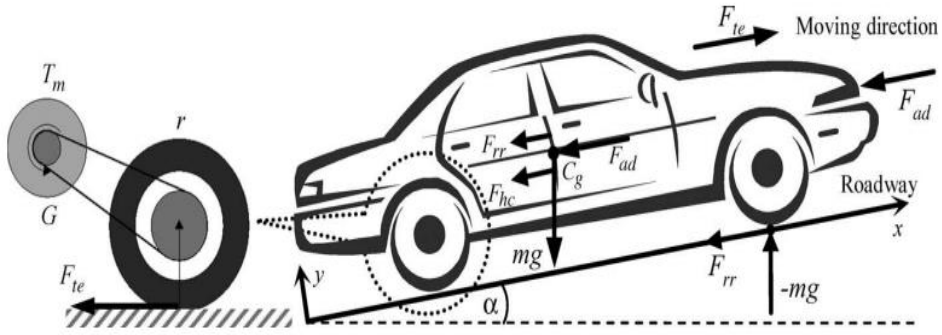

Figure 3. Mechanical forces acting on EV [18]

The power required to drive the EV at speed v must compensate for the resistive forces:

$$P = vF_{te} = v\left(\mu_{rr}mg + mg\,sin\,f + \frac{1}{2}\rho AC_d v^2 + m\frac{dv}{dt} + F_L\right) \quad (11)$$

Under the FOC strategy, the electromagnetic torque can be simplified as (12):

$$T_e = K_t i_{sq} \quad (12)$$

where K_t is the torque constant; i_{sq} is the stator current component in the dq frame.

From the vehicle dynamic model (1)–(3), the required torque of the in-wheel motor can be expressed as (13):

$$\frac{T_m}{n} = T_{motor} = K_t i_{sq} \quad (13)$$

where i_{sq} is the stator current command corresponding to the desired torque; n is the number of traction motors in the EV. The torque equation for the in-wheel SPIM is given by (14):

$$T_e = J\frac{d\omega_r}{dt} + B\omega_r + T_{motor} = J\frac{d\omega_r}{dt} + B\omega_r + \frac{T_m}{n} \quad (14)$$

where J is the moment of inertia of the in-wheel SPIM including the tire; B is the viscous coefficient. Assuming constant SPIM parameters, the overall EV dynamic model including the SPIM torque equation is written as (15a):

$$T_e = \left(J + m\frac{r^2}{nG^2}\right)\frac{d\omega_r}{dt} + B\omega_r + \frac{r}{nG}\left(\mu_{rr}mg + \frac{1}{2}\rho AC_d v^2 + mg\,sin\,\phi + F_L\right) \quad (15a)$$

Simplifying gives:

$$T_e = \left(J + m\frac{r^2}{nG^2}\right)\frac{d\omega_r}{dt} + B\omega_r + T_L \quad (15b)$$

where TL is the load torque including effects from rolling resistance, aerodynamic drag, road slope, and external disturbances.

3. THE STABS_PCH CONTROL STRUCTURE FOR FOC-BASED SPIM DRIVES

3.1. Design of the STABS controller for outer speed and flux loops

In this study, an adaptive VGSTABS approach is developed for the vector control of SPIM drives. The stability and dynamic behavior of the proposed control system are analyzed within the Lyapunov framework [14]. BS control provides a recursive procedure for constructing nonlinear control laws, where a virtual control signal is introduced to guarantee system convergence toward equilibrium. This strategy enables the design of robust controllers capable of handling various disturbances and parameter uncertainties. To further enhance robustness, integral terms of the tracking errors are incorporated into the BS design.

Moreover, the modified BS scheme is combined with the VGSTA method, which strengthens its ability to cope with parameter variations and load disturbances while effectively reducing the chattering commonly observed in conventional sliding-mode control methods.

$$\varepsilon_\omega = (\omega_r^* - \omega_r) + k_\omega \int_0^t (\omega_r^* - \omega_r)dt$$
$$\varepsilon_\psi = (\psi_{rd}^* - \psi_{rd}) + k_\psi \int_0^t (\psi_{rd}^* - \psi_{rd})dt \quad (16)$$

The error dynamical equations are

$$\dot{\varepsilon_\omega} = \dot{\omega^*} - \frac{3}{2} n_p \frac{\delta\sigma L_s}{J} \psi_{rd} i_{sq}^* + \frac{T_l}{J} + B\omega + k_\omega^{'}(\omega^* - \omega)$$
$$\dot{\varepsilon_\psi} = \dot{\psi_{rd}^*} - \frac{L_m}{\tau_r} i_{sd}^* + \frac{1}{\tau_r}\psi_{rd} + k_\psi^{'}(\psi_{rd}^* - \psi_{rd}) \quad (17)$$

To obtain the virtual controller of speed and rotor flux loop, the following Lyapunov function candidate is considered:

$$V_{(\omega,\psi)} = \frac{1}{2}\left(\varepsilon_\omega^2 + \varepsilon_\psi^2\right) \quad (18)$$

Differentiating V and combining formula (5), we get:

$$\dot{V_{(\omega,\psi)}} = \varepsilon_\omega \dot{\varepsilon_\omega} + \varepsilon_\psi \dot{\varepsilon_\psi} = \varepsilon_\omega \left[\dot{\omega^*} - k_t \psi_{rd} i_{sq} + \frac{T_I}{J} + B\omega + k_\omega^{'}(\omega^* - \omega)\right] + \varepsilon_{\psi_{rd}} \left\{\dot{\psi_{rd}^*} - \frac{L_m}{\tau_r} i_{sd}^* + \frac{1}{\tau_r}\psi_{rd} + k_\psi^{'}(\psi_{rd}^* - \psi_{rd})\right\} \quad (19)$$

where: $k\omega$, $k\Psi$ are positive constants

$$k_t = \frac{3}{2} n_p \frac{\delta\sigma L_s}{J};$$

To V' <0, the stabilizing virtual controls are chosen as (20).

$$i_{sq}^* = \frac{1}{k_t \psi_{rd}}\left\{k_\omega \varepsilon_\omega + \dot{\omega^*} + B\omega + \frac{T_l}{J} + k_\omega^{'}(\omega^* - \omega)\right\} + \nu_\alpha$$
$$i_{sd}^* = \frac{\tau_r}{L_m}\left\{k_\psi \varepsilon_\psi + \dot{\psi_{rd}^*} + \frac{1}{\tau_r}\psi_{rd} + k_\psi^{'}(\psi_{rd}^* - \psi_{rd})\right\} + \nu_\beta \quad (20)$$

where, ν_α, ν_β are the control signals injected in order to improved the performance of BS controller. The load torque T_L is estimated:

$$T_L = \frac{1}{1+\tau_0 p}\left[\left(\frac{3}{2} P \frac{L_m}{L_r} \hat{\psi_{rd}} i_{sq}\right) - \frac{J}{P}\frac{d\omega}{dt}\right]; \quad (21)$$

where: τ0: is time gain; p: differential.

The variable-gain second-order sliding mode strategy adjusts its gain based on the real disturbance bound, thereby mitigating the intensity of chattering. In this framework, the super-twisting algorithm is enhanced with a variable-gain mechanism to compensate for disturbances whose gradient bounds depend on the system states.

According to [30]–[32], the proposed variable-gain super-twisting algorithm (VGSTA) is formulated as (22):

$$\begin{cases} v_1(t) = k_\omega(t, \varepsilon_\omega)\left[\delta_1 \phi_{\omega 1}(S_1) + \mu_1 \int_0^t \phi_{\omega 2}(S_1)dt\right] \\ v_2(t) = k_\psi(t, \varepsilon_\psi)\left[\delta_2 \phi_{\psi 1}(S_2) + \mu_2 \int_0^t \phi_{\psi 2}(S_2)dt\right] \end{cases} \quad (22)$$

$$\text{where, } \begin{cases} k_{\alpha\omega}(t,\varepsilon\omega) = S_1 sat(S_1) \\ k_{\alpha\psi}(t,\varepsilon\psi) = S_2 sat(S_2) \\ \phi_1(S_x) = |S_x|^{\frac{1}{2}} sat(S_x) + k_3 S_x \\ \quad \phi_2(S_x) = \frac{1}{2} sat(S_x) + \frac{3}{2} k_3 |S_x|^{\frac{1}{2}} sat(S_x) + k_3^2 S_x \end{cases} \tag{23}$$

From (19)-(20) and (22)-(23), we obtain:

$$\frac{dV(\omega,\psi)}{dt} = -k_\omega \varepsilon_\omega^2 - k_\psi \varepsilon_\psi^2 - \varepsilon_\omega \nu_\alpha - \varepsilon_\psi \nu_\beta < 0 \tag{24}$$

The virtual controls in (20) are chosen to satisfy the control objectives and also provide references for the next step of the VGSTA SM controller design.

3.2. SMC design with the variable-gain super-twisting algorithm for in the inner current loops

In this part, a high-order nonlinear sliding control algorithm based on Lyapunov stability theory using the variable-gain super-twisting algorithm is proposed for the inner current loops to increase robustness of overall system, minimizing the effects of parameter variations and unforeseen disturbances in the control process. The current error tracking function defined:

$$\varepsilon_{isd} = i_{sd}^* - i_{sd}; \qquad \varepsilon_{isq} = i_{sq}^* - i_{sq} \tag{25}$$

The corresponding nonlinear slip surface according to the current components is defined as (26):

$$\begin{cases} S_3 = \varepsilon_{\mathrm{isd}} + k_4 |\int \varepsilon_{\mathrm{isd}} dt|^{\frac{1}{2}} sat(\int \varepsilon_{\mathrm{isd}} dt) \\ S_4 = \varepsilon_{\mathrm{isq}} + k_5 |\int \varepsilon_{\mathrm{isq}} dt|^{\frac{1}{2}} sat(\int \varepsilon_{\mathrm{isq}} dt) \end{cases} \tag{26}$$

Combining formula (5), taking the time differential on both sides of (26), we get:

$$\begin{aligned} \frac{dS_3}{dt} &= \frac{d\varepsilon_{\mathrm{isd}}}{dt} + \frac{d}{dt}\left[k_4 \left|\int \varepsilon_{\mathrm{isd}} dt\right|^{\frac{1}{2}} sat\left(\int \varepsilon_{\mathrm{isd}} dt\right)\right] \\ &= \frac{di_{sd}^*}{dt} - \frac{1}{L_s}\left[-\mathrm{ai_{sd}} + \mathrm{L}_s \omega_e i_{\mathrm{sq}} + \mathrm{bR}_r \psi_{\mathrm{rd}} + \mathrm{cu_{sd}}\right] + \frac{d}{dt}\left[k_4 |\int \varepsilon_{\mathrm{isd}} dt|^{\frac{1}{2}} sat(\int \varepsilon_{\mathrm{isd}} dt)\right] = -v_3 \\ \frac{dS_4}{dt} &= \varepsilon_{\mathrm{isq}} + k_5 \left|\int \varepsilon_{\mathrm{isq}} dt\right|^{\frac{1}{2}} sat\left(\int \varepsilon_{\mathrm{isq}} dt\right) \\ &= \frac{di_{sq}^*}{dt} - \frac{1}{L_s}\left[-\mathrm{ai_{sq}} - \mathrm{L}_s \omega_e i_{\mathrm{sd}} - \mathrm{b}_r \omega_e \psi_{\mathrm{rd}} + \mathrm{cu_{sq}}\right] + \frac{d}{dt}\left[k_5 \left|\int \varepsilon_{\mathrm{isq}} dt\right|^{\frac{1}{2}} sat\left(\int \varepsilon_{\mathrm{isq}} dt\right)\right] = -v_4 \end{aligned} \tag{27}$$

In the proposed method, we select the ν_3 and ν_4 switching control functions, based on the design principles presented in

$$\begin{cases} v_3(t) = k_{\alpha 1}(t, \varepsilon_{\mathrm{isd}}) \left[\delta_1 \phi_1(S_3) + \mu_1 \int_0^t \phi_2(S_3) dt\right] \\ v_4(t) = k_{\alpha 2}(t, \varepsilon_{\mathrm{isq}}) \left[\delta_2 \phi_1(S_4) + \mu_2 \int_0^t \phi_2(S_4) dt\right] \end{cases} \tag{28}$$

$$\text{where, } \begin{cases} k_{\alpha 1}(t, \varepsilon_{\mathrm{isd}}) = S_3 sat(S_3) \\ k_{\alpha 2}(t, \varepsilon_{\mathrm{isq}}) = S_4 sat(S_4) \\ \phi_1(S_x) = |S_x|^{\frac{1}{2}} sat(S_x) + k_6 S_x \\ \quad \phi_2(S_x) = \frac{1}{2} sat(S_x) + \frac{3}{2} k_6 |S_x|^{\frac{1}{2}} sat(S_x) + k_6^2 S_x \end{cases} \tag{29}$$

With *x=1:2, k4, k5, k6, δ1, δ2, μ1, μ2* are positive coefficients. From (27) the virtual control functions of the current control loop are determined as follows:

$$\begin{cases} u_{sd}^{*} = \frac{L_s}{c}\left\{v_3(t) + \frac{di_{sd}^{*}}{dt} + \frac{d}{dt}\left[k_4\left|\int \varepsilon_{\mathrm{isd}} dt\right|^{\frac{1}{2}} sat\left(\int \varepsilon_{\mathrm{isd}} dt\right)\right]\right\} \\ \quad + \frac{1}{c}\left[\mathrm{ai_{sd}} - \mathrm{L_s}\omega_e i_{\mathrm{sq}} - \mathrm{bR}_r\psi_{\mathrm{rd}}\right] \\ u_{sq}^{*} = \frac{L_s}{c}\left\{v_4(t) + \frac{di_{sq}^{*}}{dt} + \frac{d}{dt}\left[k_5\left|\int \varepsilon_{\mathrm{isq}} dt\right|^{\frac{1}{2}} sat\left(\int \varepsilon_{\mathrm{isq}} dt\right)\right]\right\} \\ \quad + \frac{1}{c}\left[\mathrm{ai_{sq}} + \mathrm{L_s}\omega_e i_{\mathrm{sd}} + \mathrm{b}_r\omega_e\psi_{\mathrm{rd}}\right] \end{cases} \quad (30)$$

We select the Lyapunov function:

$$V = \frac{1}{2}[S_3^2 + S_4^2] \quad (31)$$

Differentiate both sides of (31), combine with formulas (27) and (28) to get:

$$\begin{aligned} \frac{dV}{dt} &= S_3\frac{dS_3}{dt} + S_4\frac{dS_4}{dt} \\ &= -k_{\alpha 1}(t, \varepsilon_{\mathrm{isd}})S_1\left[\phi_1(S_3) + \int_0^t \phi_2(S_3)dt\right] - k_{\alpha 2}(t, \varepsilon_{\mathrm{isq}})S_4\left[\phi_1(S_4) + \int_0^t \phi_2(S_4)dt\right] \end{aligned} \quad (32)$$

From (32), we see that the differential of the Lyapunov function is always negative. Therefore, the system is always stable.

4. SIMULATION AND DISCUSSION

To validate the effectiveness and robustness of the proposed IABSSOSM control strategy, detailed simulations were conducted using MATLAB/Simulink on an electric vehicle (EV) propulsion system driven by a six-phase induction motor (SPIM). The primary objective of this simulation study is to assess the dynamic performance, reference speed tracking accuracy, torque response quality, and robustness against disturbances and parameter variations. Figure 4 illustrates the complete FOC-based vector control system utilizing the proposed hybrid structure.

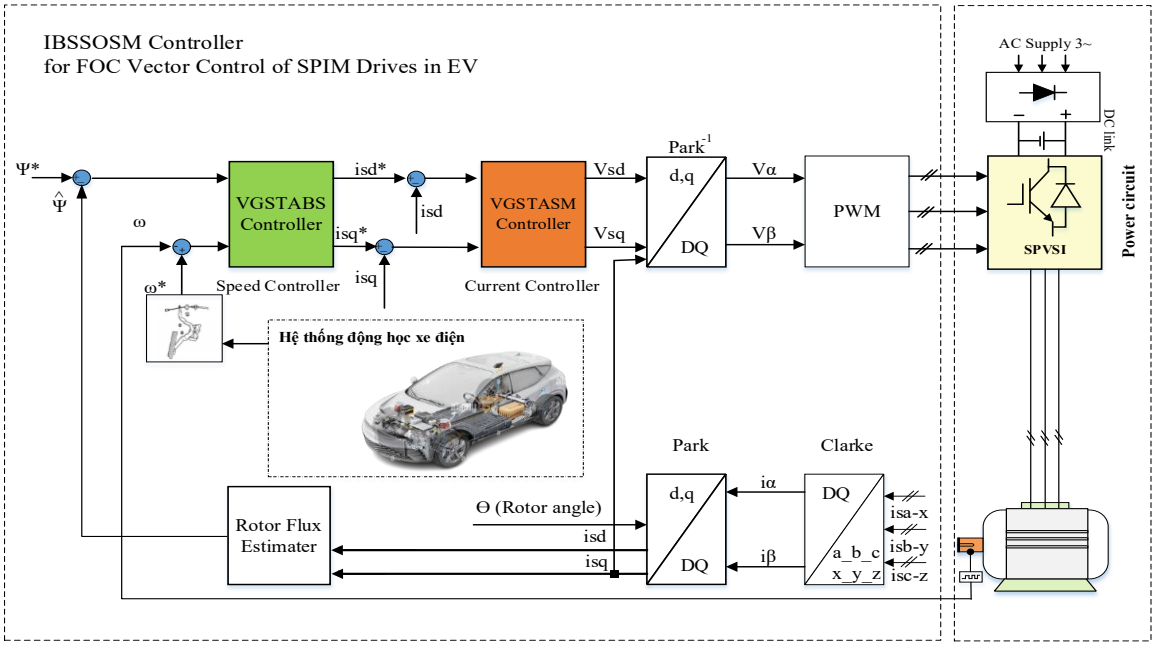

Figure 4. FOC vector control of SPIM drive using novel improved BS_SM control structure

The test profiles include a modified ECE-40 urban driving cycle, an enhanced ECE-15 cycle, and a step speed reference profile, based on standard drive patterns from [2], [11], [18], and [25]. The SPIM motor

parameters used are: 10 kW, 220 V, 50 Hz, 6 poles, 970 rpm. Electrical parameters: 10 kW, 220 V, 50 Hz, 6 pole, 970 rpm. Rs=1.63Ω, Rr=1.08Ω, Ls=0.2792 H, Lr=0.2602 H, Lm=0,2602 H, J=0.109 kg.m2.

4.1. Test case 1 – modified ECE-40 urban driving cycle

This test evaluates system behavior under a modified ECE-40 urban cycle, based on [25], simulating low-speed city driving (0–55 km/h). As shown in Figure 5, the proposed controller demonstrates accurate reference tracking, rapid torque response, and stable rotor flux regulation during frequent acceleration and deceleration phases. The EV's speed closely tracks the reference, with negligible error in both transient and steady-state phases—even at very low or zero speeds. Torque response is fast and stable; rotor flux is well maintained. The IABSSOSM controller delivers excellent performance during both acceleration and deceleration, ensuring timely speed adjustments.

These results confirm the IABSSOSM controller's ability to maintain speed accuracy with minimal overshoot and smooth current transitions under complex, stop-and-go city conditions. Compared to PID or BS-SMC controllers, the proposed method provides enhanced convergence and improved chattering suppression. Especially beneficial at low speeds where EV torque control is most sensitive.

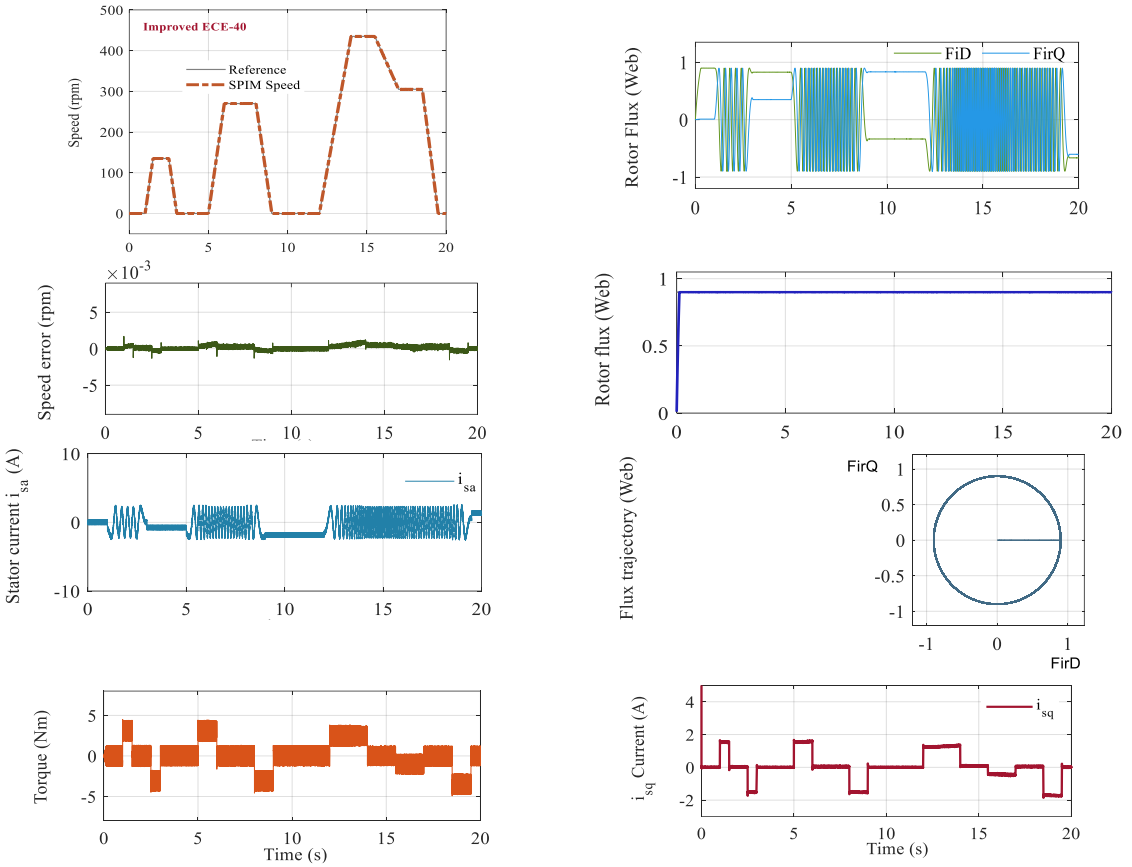

Figure 5. Speed response, current, rotor flux, and torque under the modified ECE-40 cycle [25]

4.2. Test case 2_extended urban cycle – enhanced ECE-15

In the second scenario, the system is subjected to a modified ECE-15 profile over five cycles, includes four low-speed and one high-speed segment. This test uses a pattern similar in [18], it is useful for validating EV performance in urban, suburban, and highway scenarios. Figure 6 shows speed response, current, and torque.

Observations these results in Figure 6, it is easy to see that, speed closely follows the reference across all phases. Transient process is managed without oscillations or delay. Torque peaks are appropriately damped due to predictive estimation. The VGSTA mechanism enables gain adaptation under time-varying load disturbances, an improvement over fixed-gain designs commonly used in past literature. This improve provides the controller's adaptability and robustness in dynamic and prolonged driving conditions.

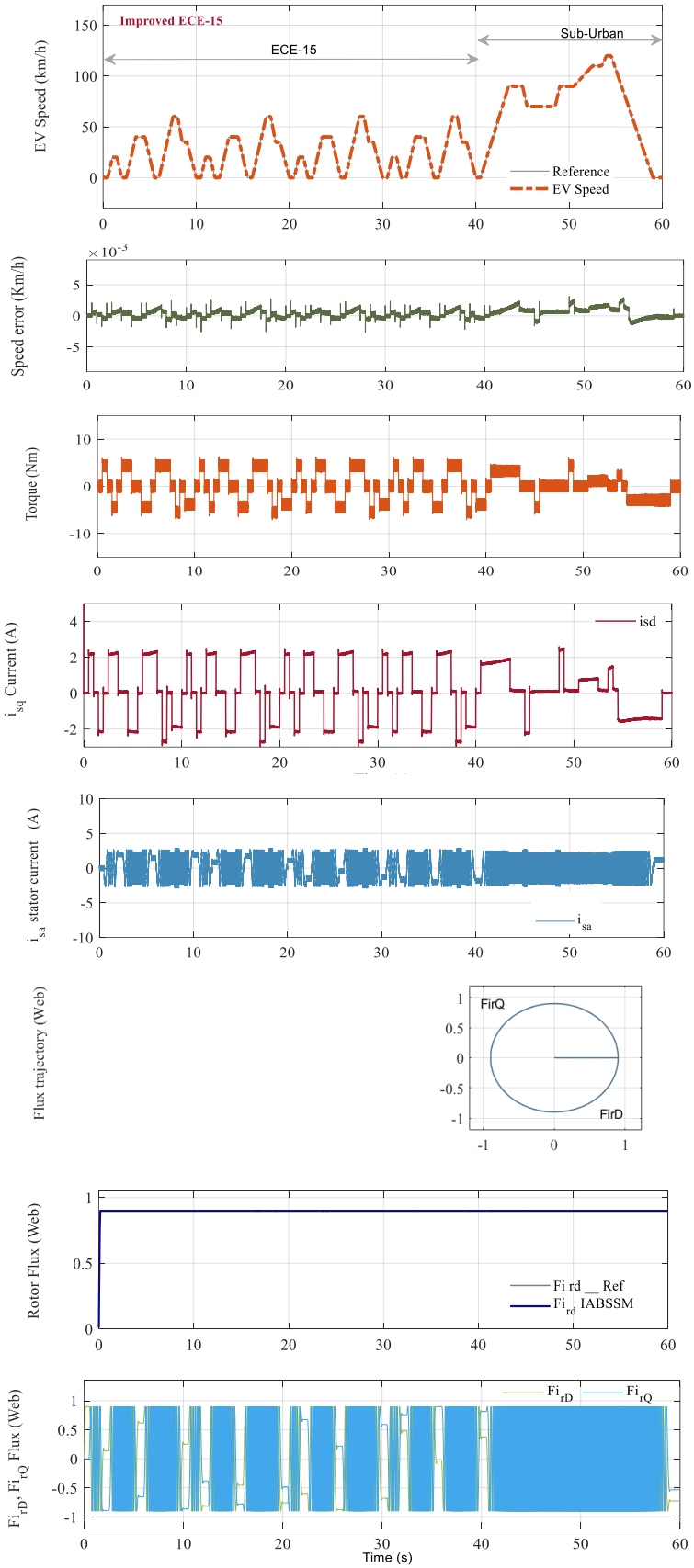

Figure 6. Speed, speed error, current, and torque response in the enhanced ECE-15 test cycle

4.3. Test case 3 – step speed reference tracking

To further investigate the transient performance and adaptability under abrupt setpoint changes, a step-reference speed profile is applied. The vehicle accelerates from 0 to 60 km/h (~400 rpm), then, decelerates to 30 km/h (~200 rpm), and then accelerates to 80 km/h (~535 rpm) simulating flat, downhill, and uphill driving scenarios. This test is based on the drive model from [2].

Figure 7 shows speed, stator current, and torque during the full test. The results verify that the proposed controller offers fast dynamic response and excellent control quality across both steady and transient states—satisfying EV propulsion requirements under all operating conditions. Across all three test cases, the reference tracking error remains near zero in steady-state. The IABSSOSM controller provides responsive and accurate control during both acceleration and deceleration phases. The control signals are derived based on the Lyapunov theory ensures stable system operation. Current and flux are tightly regulated in all three test scenarios.

In the third test case, due to the step-type reference input, current and torque peaks occur at the transition points, but they quickly converge to the desired values. Estimation and tracking errors approach zero in steady-state. As presented in Figure 7, the controller quickly tracks each reference transition with minimal overshoot (<3%) and settling time (<0.15s). Torque and current transients remain well within operational bounds and quickly stabilize after each change. Rotor flux maintains constant amplitude, indicating strong magnetic stability.

It is clear that, this scenario is critical for EVs, especially during aggressive maneuvers or changes in driver commands. The proposed controller handles all speed jumps smoothly without requiring controller retuning or prior disturbance knowledge. The VGSTA effectively modulates the control effort based on error magnitude and disturbance estimate, ensuring finite-time convergence. These features mark a substantial improvement over classical SMC which often suffers from chattering at high gains and poor convergence when gains are fixed.

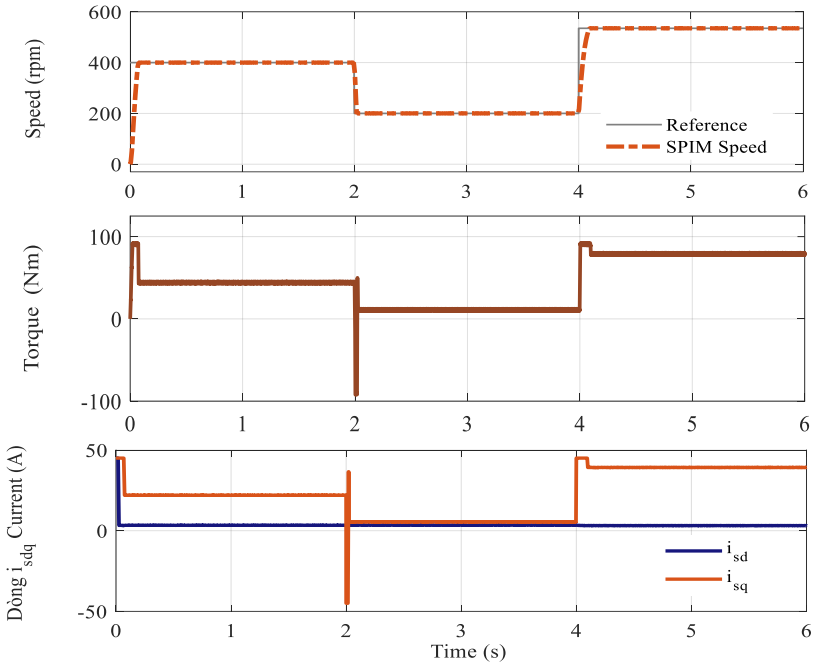

Figure 7. Speed response, torque and ISDQ current under sudden changes in reference speed

4.4. Robustness evaluation under step load disturbance

A step torque disturbance is introduced at zero-speed to assess load rejection capabilities in Test 4. This test is conducted based on the reference implementation in [11]. Figure 8 illustrates the system response in terms of speed tracking, estimation error, stator current, rotor flux, and electromagnetic torque. The obtained results show that despite a sudden increase in external torque, the system maintains speed at 0 km/h, and rotor flux and current remain stable these demonstrate the high accuracy of the controller.

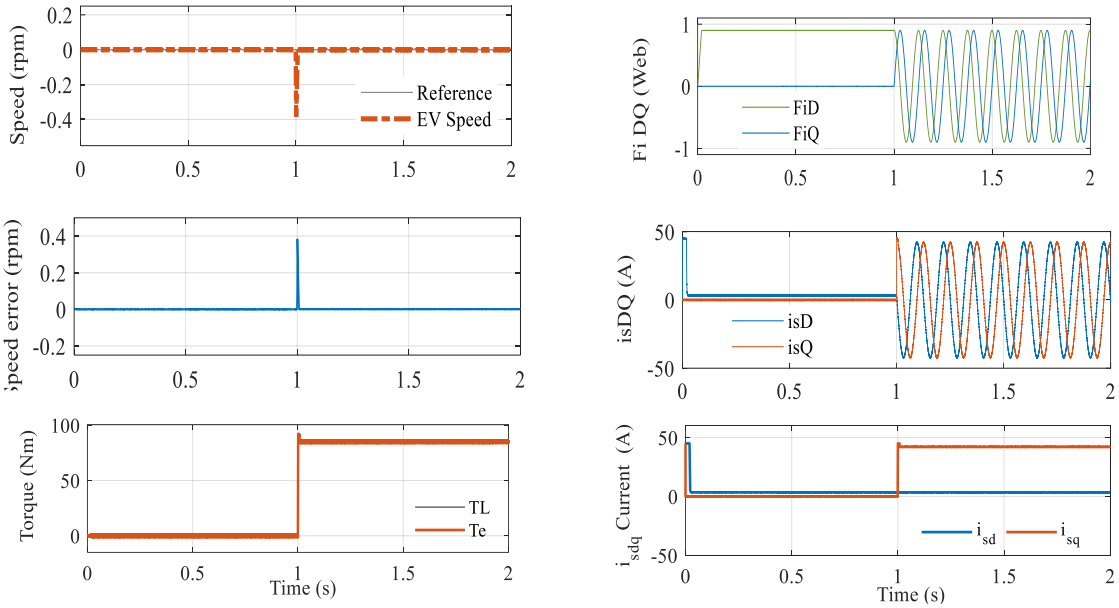

Figure 8. Speed response, estimation error, current, and torque based on the test in [11]

By integrating VGSTA and predictive estimation, this work addresses two major weaknesses of prior BS-SMC structures: fixed gain tuning and lack of foresight in disturbance rejection. These improvements offer real-world applicability, particularly in EVs requiring adaptive control under dynamic urban and highway conditions. The system demonstrates excellent dynamic behavior, high tracking precision, and robust torque response in four tests. These results valid the proposed controller's ability to maintain system stability and performance under variable operating conditions. While simulation results are promising, experimental validation on a physical EV platform is required to assess real-time performance under sensor noise and inverter nonlinearity. Future research will extend this work to Hardware-in-the-Loop simulation and embedded implementation using DSP or FPGA platforms.

5. CONCLUSION

This paper has proposed a novel field-oriented control strategy for the speed control of a dual-star six-phase induction motor (DSIM) applied to EV drive systems. The control structure integrates a hybrid nonlinear controller and variable -gain- super-twisting algorithm. In addition, a predictive torque estimator is introduced to proactively reject external disturbances and further enhance the performance of the IABSSOSM control framework. The developed control scheme demonstrates precise reference speed tracking, fast torque response, and high operational reliability under varying load conditions. The proposed EV drive control system fulfills key technical requirements, including a wide speed regulation range, rapid startup capability, and stable low-speed operation under high torque demand. Simulation results validate the effectiveness of the IABSSOSM strategy and confirm its suitability for real-world EV applications, aligning with industry expectations and performance standards. In future work, the proposed IABSSOSM controller will be implemented on real-time embedded platforms and validated through hardware. Further research will develop its application to multi-motor EV systems to enhance coordination and robustness in practical environments.

FUNDING INFORMATION

Authors state no funding involved.

AUTHOR CONTRIBUTIONS STATEMENT

This journal uses the Contributor Roles Taxonomy (CRediT) to recognize individual author contributions, reduce authorship disputes, and facilitate collaboration.

Name of Author	C	M	So	Va	Fo	I	R	D	O	E	Vi	Su	P	Fu
Huu Dat Tran		✓	✓	✓	✓	✓		✓	✓	✓	✓			
Ngoc Thuy Pham	✓	✓	✓	✓	✓	✓		✓	✓	✓		✓	✓	

C : **C**onceptualization
M : **M**ethodology
So : **So**ftware
Va : **Va**lidation
Fo : **Fo**rmal analysis
I : **I**nvestigation
R : **R**esources
D : **D**ata Curation
O : Writing - **O**riginal Draft
E : Writing - Review & **E**diting
Vi : **Vi**sualization
Su : **Su**pervision
P : **P**roject administration
Fu : **Fu**nding acquisition

CONFLICT OF INTEREST STATEMENT

Authors state no conflict of interest.

REFERENCES

[1] M. K. B. Boumegouas and K. Kouzi, "A new synergetic scheme control of electric vehicle propelled by six-phase permanent magnet synchronous motor," *Advances in Electrical and Electronic Engineering*, vol. 20, no. 1, pp. 1–14, 2022, doi: 10.15598/aeee.v20i1.4221.

[2] D. H. Park *et al.*, "Magnetizing inductance estimation method of induction motor for EV traction considering magnetic saturation changes according to current and slip frequency," *IEEE Transactions on Magnetics*, vol. 60, no. 9, 2024, doi: 10.1109/TMAG.2024.3426663.

[3] B. Gasbaoui, A. Nasri, and O. Abdelkhalek, "An efficiency PI speed controller for future electric vehicle in several topology," *Procedia Technology*, vol. 22, pp. 501–508, 2016, doi: 10.1016/j.protcy.2016.01.109.

[4] Y. Bensalem, A. Kouzou, R. Abbassi, H. Jerbi, R. Kennel, and M. Abdelrahem, "Sliding-mode-based current and speed sensors fault diagnosis for five-phase pmsm," *Energies*, vol. 15, no. 1, 2022, doi: 10.3390/en15010071.

[5] M. K. Islam, M. Karimi-Ghartemani, and S. Choi, "Design of a robust optimal controller for five-phase permanent magnet assisted synchronous reluctance motor in electric vehicle application," in *Conference Proceedings - IEEE Applied Power Electronics Conference and Exposition - APEC*, 2021, pp. 1078–1085. doi: 10.1109/APEC42165.2021.9487435.

[6] G. Sifelislam, T. Bekheira, N. Kamal, N. Mokhtar, and A. Idir, "Virtual vector-based neural network DTC scheme for dynamic performance improvement of dual-star induction motor drive," *e-Prime - Advances in Electrical Engineering, Electronics and Energy*, vol. 11, p. 100938, 2025, doi: 10.1016/j.prime.2025.100938.

[7] N. T. Pham, "Design of Novel STASOSM Controller for FOC Control of Dual Star Induction Motor Drives," *International Journal of Robotics and Control Systems*, vol. 4, no. 3, pp. 1059–1074, 2024, doi: 10.31763/ijrcs.v4i3.1443.

[8] E. Levi, M. Jones, and D. Dujic, *Electric multiphase motor drives: Modeling and control*. CRC Press, 2020.

[9] A. Chantoufi *et al.*, "Direct torque control-based backstepping speed controller of doubly fed induction motors in electric vehicles: Experimental validation," *IEEE Access*, vol. 12, pp. 139758–139772, 2024, doi: 10.1109/ACCESS.2024.3462821.

[10] Q. Al Azze and I. A. R. Hameed, "Reducing torque ripple of induction motor control via direct torque control," *International Journal of Electrical and Computer Engineering*, vol. 13, no. 2, pp. 1379–1386, 2023, doi: 10.11591/ijece.v13i2.pp1379-1386.

[11] E. Zerdali and R. Demir, "Speed-sensorless predictive torque controlled induction motor drive with feed-forward control of load torque for electric vehicle applications," *Turkish Journal of Electrical Engineering and Computer Sciences*, vol. 29, no. 1, pp. 223–240, 2021, doi: 10.3906/ELK-2005-75.

[12] A. Das and S. Chatterjee, "A novel speed sensor-less stator flux-oriented vector control of dual-stator induction generator for grid-tied wind energy conversion system," *International Journal of Circuit Theory and Applications*, vol. 53, no. 1, pp. 380–408, 2025, doi: 10.1002/cta.4070.

[13] P. T. M. Sahridayan and R. Gopal, "Modeling and analysis of field-oriented control based permanent magnet synchronous motor drive system using fuzzy logic controller with speed response improvement," *International Journal of Electrical and Computer Engineering*, vol. 12, no. 6, pp. 6010–6021, 2022, doi: 10.11591/ijece.v12i6.pp6010-6021.

[14] B. Abdellah, K. Medjdoub, A. Hazzab, H. Trabelsi, M. Rezkallah, and A. Chandra, "Control of PMSM drives for EV using nonlinear techniques and input-output linearization," in *2024 2nd International Conference on Electrical Engineering and Automatic Control, ICEEAC 2024*, 2024, pp. 1–4. doi: 10.1109/ICEEAC61226.2024.10576460.

[15] B. Benbouya *et al.*, "Sliding mode control of an electric vehicle driven by a new powertrain technology based on a dual-star induction machine," *World Electric Vehicle Journal*, vol. 15, no. 4, p. 155, 2024, doi: 10.3390/wevj15040155.

[16] C. P. Gor, V. A. Shah, and B. Rangachar, "Fuzzy logic based dynamic performance enhancement of five phase induction motor under arbitrary open phase fault for electric vehicle," *International Journal of Emerging Electric Power Systems*, vol. 22, no. 4, pp. 473–492, 2021, doi: 10.1515/ijeeps-2020-0271.

[17] A. Mousaei, N. Rostami, and M. B. Bannae Sharifian, "Design a robust and optimal fuzzy logic controller to stabilize the speed of an electric vehicle in the presence of uncertainties and external disturbances," *Transactions of the Institute of Measurement and Control*, vol. 46, no. 3, pp. 482–500, 2024, doi: 10.1177/01423312231178169.

[18] A. Haddoun, M. E. H. Benbouzid, D. Diallo, R. Abdessemed, J. Ghouili, and K. Srairi, "Modeling, analysis, and neural network control of an EV electrical differential," *IEEE Transactions on Industrial Electronics*, vol. 55, no. 6, pp. 2286–2294, 2008, doi: 10.1109/TIE.2008.918392.

[19] S. Suganthi and R. Karpagam, "Dynamic performance improvement of PMSM drive using fuzzy-based adaptive control strategy for EV applications," *Journal of Power Electronics*, vol. 23, no. 3, pp. 510–521, 2023, doi: 10.1007/s43236-023-00594-3.

[20] N. T. Pham and P. D. Nguyen, "A novel hybrid backstepping and fuzzy control for three phase induction motor drivers," *International Journal of Robotics and Control Systems*, vol. 5, no. 1, pp. 599–610, 2025, doi: 10.31763/ijrcs.v5i1.1707.

[21] K. Mathew K, D. M. Abraham, and A. Harish, "Speed regulation of PMSM drive in electric vehicle applications with sliding mode controller based on Harris Hawks optimization," *e-Prime - Advances in Electrical Engineering, Electronics and Energy*, vol. 9, p. 100643, 2024, doi: 10.1016/j.prime.2024.100643.

[22] A. Ghezouani, I. S. Bousmaha, and J. Ghouili, "SMO based sensorless direct torque sliding mode control of IM for EV

applications," in *ICAEE 2024 - International Conference on Advanced Electrical Engineering 2024*, 2024, pp. 1–7. doi: 10.1109/ICAEE61760.2024.10783193.
[23] C. Yin, Y. Xie, D. Shi, S. Wang, K. Zhang, and M. Li, "Sliding mode coordinated control of hybrid electric vehicle via finite-time control technique," *ISA Transactions*, vol. 146, pp. 541–554, 2024, doi: 10.1016/j.isatra.2024.01.014.
[24] C. Qiao, W. Sun, and Q. Zhang, "A Hamiltonian-based method for PMSM in electric vehicle considering iron loss and saturation," *International Journal of Control, Automation and Systems*, vol. 22, no. 8, pp. 2385–2393, 2024, doi: 10.1007/s12555-022-0927-5.
[25] F. J. Lin, Y. C. Hung, J. C. Hwang, I. P. Chang, and M. T. Tsai, "Digital signal processor-based probabilistic fuzzy neural network control of in-wheel motor drive for light electric vehicle," *IET Electric Power Applications*, vol. 6, no. 2, pp. 47–61, 2012, doi: 10.1049/iet-epa.2011.0153.
[26] E. Touti, M. Aoudia, C. H. Hussaian Basha, and I. M. Alrougy, "A novel design and analysis adaptive hybrid ANFIS MPPT controller for PEMFC-fed EV systems," *International Transactions on Electrical Energy Systems*, vol. 2024, p. 5541124, 2024, doi: 10.1155/2024/5541124.
[27] K. Abed and H. K. E. Zine, "Intelligent fuzzy back-stepping observer design based induction motor robust nonlinear sensorless control," *Electrical Engineering and Electromechanics*, vol. 2024, no. 2, pp. 10–15, 2024, doi: 10.20998/2074-272X.2024.2.02.
[28] W. Wang, Y. Ye, X. Chen, and Y. Yuan, "Adaptive high-order sliding-mode low-speed control with RBF neural network nonlinear disturbance observer for PMSM drive system," *IEEE Transactions on Power Electronics*, vol. 40, no. 8, pp. 10865–10876, 2025, doi: 10.1109/TPEL.2025.3559890.
[29] N. T. Pham, "Speed tracking of field oriented control SPIM drive using (BS_SOSM) nonlinear control structure," *WSEAS Transactions on Systems and Control*, vol. 14, pp. 291–299, 2019.
[30] N. Derbel, J. Ghommam, and Q. Zhu, Eds., *Applications of sliding mode control*, vol. 79. Singapore: Springer Singapore, 2017. doi: 10.1007/978-981-10-2374-3.
[31] Y. Shtessel, C. Edwards, L. Fridman, and A. Levant, *Sliding mode control and observation*. Springer, 2014. doi: 10.1007/978-0-8176-4893-0.
[32] L. Fridman, J. P. Barbot, and F. Plestan, *Recent trends in sliding mode control*. The Institution of Engineering and Technology, 2016. doi: 10.1049/PBCE102E.

BIOGRAPHIES OF AUTHORS

Huu Dat Tran received the engineer's degree in electrical and electronic engineering from Electric Power University, Vietnam, in 2022. He is currently working at the Southern Electrical Testing Company. Since 2023, he has been pursuing the master's degree at Ho Chi Minh City University of Industry. His research interests include AC motor drives, multiphase motors, renewable energy, and intelligent control. He can be contacted at 22734111.dat@student.iuh.edu.vn.

Ngoc Thuy Pham is currently with the Industrial University of Ho Chi Minh City (IUH), Ho Chi Minh City, Vietnam. She received the B.Sc. degree in Electrical Engineering from Thai Nguyen University of Technology, Vietnam, in 1994, the M.Sc. degree in electrical engineering from Ho Chi Minh City University of Technology (HCMUT), Vietnam, in 2009, and the Ph.D. degree in control engineering and automation from Ho Chi Minh City University of Transport, Vietnam, in 2020. Her current research interests include AC motor drives, nonlinear and intelligent control. She can be contacted at phamthuyngoc@iuh.edu.vn.